Inorg. Chem. **2004**, *43*, 7301–7307

Synthesis, Structure, and Cooperative Proton–Electron Transfer Reaction of Bis(5,6-diethylpyrazinedithiolato)metal Complexes (M = Ni, Pd, Pt)

Takashi Kubo,*,† Misako Ohashi,† Katsuaki Miyazaki,† Akio Ichimura,‡ and Kazuhiro Nakasuji*,†

Department of Chemistry, Graduate School of Science, Osaka University, Machikaneyama 1-1, Toyonaka, Osaka 560-0043, Japan, and Graduate School of Science, Osaka City University, Sumiyoshi-ku, Osaka 558-8585, Japan

Received March 22, 2004

New proton and electron donors, $M^{II}(HL)_2$ (M = Ni, Pd, Pt; L = 5,6-diethylpyradzinedithiolate), as well as a proton and electron acceptor, $Pt^{IV}(L)_2$, were prepared and characterized. The pH-dependent cyclic voltammetry of the $M^{II}(HL)_2$ complexes revealed a favorable Gibbs free energy ($K_{com} > 1$) for the proton and electron transfer reactions from $M^{II}(HL)_2$ to $M^{IV}(L)_2$; i.e., the equilibrium for the following reaction lies to the right: $M^{II}(HL)_2 + M^{IV}(L)_2 \rightleftarrows 2M^{III}(HL)(L)$.

Introduction

Cooperative phenomena of proton and electron transfer are of great interest not only from a scientific but also from a new-material point of view.[1] As previously reported, we have investigated the cooperative proton and electron transfer (PET) systems based on hydrogen-bonded charge-transfer complexes.[2] Among these materials, hydroquinone−benzoquinone systems showed unique solid-state properties that originated from both proton and electron transfers under high pressure, characterized by pressure-dependent IR and UV spectra.[2a−c] To generate the PET phenomena under milder conditions, we have modified the conjugated rings by extending the conjugated system[2a] and by introducing donor and acceptor groups[2b] to enhance the thermodynamic and kinetic stabilities of the PET states. Although such molecular designs certainly led to a new family of PET systems, a high pressure was still required to observe the transition to the PET state.

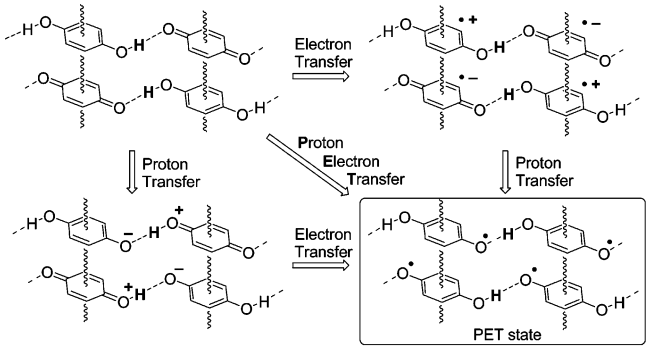

The approach in our new design to stabilize the PET state is the incorporation of transition metal atoms into molecular conjugated systems for utilizing a variety of redox states of metal atoms. We focus on transition metal complexes equipped with dissociative protons. Such metal complexes are known to exhibit pH-dependent metal-based redox properties.[3] The pH dependency of the redox potentials

* Authors to whom correspondence should be addressed. E-mail: kubo@chem.sci.osaka-u.ac.jp (T.K.).
† Osaka University.
‡ Osaka City University.

(1) (a) Decornez, H.; Hammes-Schiffer, S. *J. Phys. Chem. A* **2000**, *104*, 9370−9384. (b) Soper, J. D.; Mayer, J. M. *J. Am. Chem. Soc.* **2003**, *125*, 12217−12229. (c) Mayer, J. M.; Hrovat, D. A.; Thomas, J. L.; Borden, W. T. *J. Am. Chem. Soc.* **2002**, *124*, 11142−11147. (d) Eichem, Y.; Lehn, J.-M.; Scherl, M.; Haarer, D.; Fischer, J.; DeCian, A.; Corval, A.; Trommsdorff, H. P. *Angew. Chem., Int. Ed. Engl.* **1995**, *34*, 2530−2533. (e) Felderhoff, M.; Steller, I.; Reyes-Arellano, A.; Boese, R.; Sustmann, R. *Adv. Mater.* **1996**, *8*, 402−405. (f) Haga, M.; Ali, M. M.; Arakawa, R. *Angew. Chem., Int. Ed. Engl.* **1996**, *35*, 76−78.

(2) (a) Nakasuji, K.; Sugiura, K.; Kitagawa, T.; Toyoda, J.; Okamoto, H.; Okaniwa, K.; Mitani, T.; Yamamoto, H.; Murata, I.; Kawamoto, A.; Tanaka, J. *J. Am. Chem. Soc.* **1991**, *113*, 1862−1864. (b) Sugiura, K.; Toyoda, J.; Okamoto, H.; Okaniwa, K.; Mitani, T.; Kawamoto, A.; Tanaka, J.; Nakasuji, K. *Angew. Chem., Int. Ed. Engl.* **1992**, *31*, 852−854. (c) Mitani, T.; Saito, G.; Urayama, H. *Phys. Rev. Lett.* **1988**, *60*, 2299−2302. (d) Itoh, T.; Toyoda, J.; Tadokoro, M.; Kitagawa, H.; Mitani, T.; Nakasuji, K. *Chem. Lett.* **1995**, 41−42.

(3) (a) Slattery, S. J.; Blaho, J. K.; Lehnes, J.; Goldsby, K. A. *Coord. Chem. Rev.* **1998**, *174*, 391−416. (b) Baitalik, S.; Florke, U.; Nag, K. *Inorg. Chem.* **1999**, *38*, 3296−3308. (c) Binstead, R. A.; Meyer, T. J. *J. Am. Chem. Soc.* **1987**, *109*, 3287−3297.

10.1021/ic049621+ CCC: $27.50
Published on Web 10/16/2004

Scheme 1. Synthesis of **1**−**4**[a]

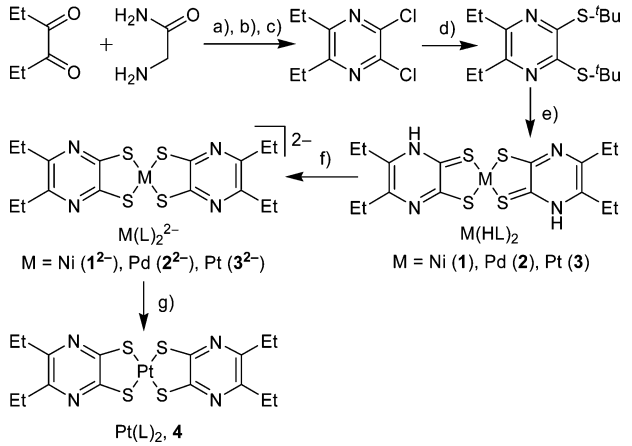

[a] Conditions: (a) NaOH, MeOH, H_2O, 28%; (b) Br_2, pyridine, AcOH, 72%; (c) $POCl_3$, pyridine, 81%; (d) *t*-BuSH, NaH, DMF, 79%; (e) $NiBr_2$, $PdCl_2$, or K_2PtCl_4, concentrated HCl, $MeOCH_2CH_2OH$; (f) NaOH, Bu_4NCl, H_2O, quantitative; (g) DDQ, CH_2Cl_2, 79%.

suggests the cooperativity between the proton and the electron. Since our ultimate aim is to understand the effects of dynamic proton displacement on solid-state properties,[4] we have decided to focus our work on square planar complexes of the Ni group. Related complexes with similar structures have been shown to possess desirable electroconductive properties in the solid state.[5] As a first step, we have estimated the thermodynamic stability of the proton and electron transfer state of the designed molecules in solution. In this study, we present the synthesis and the equilibrium constants for the proton and electron transfer reactions of (pyrazinedithiolato)metal complexes with a planar structure.

Results and Discussion

Synthesis, Structure, and Properties of Proton and Electron Donors 1−**3.** Metal complexes **1**−**3**, which were expected to behave as proton and electron donors, were prepared[6] according to the procedure outlined in Scheme 1. All the metal complexes **1**−**3** gave X-ray-quality single crystals from *N*,*N*-dimethylformamide (DMF) or *N*,*N*-dimethylacetoamide (DMAC) solutions. These compounds showed a square planar coordination and formed hydrogen bonds between an N−H site and an oxygen atom of the solvents. Two ligands of Ni complex **1** adopted trans and cis configurations incorporating DMF and DMAC, respectively (Figure 1). Pd and Pt complexes, **2** and **3**, adopted a cis configuration for the two ligands solvated with DMAC. The bond lengths and angles for **1**−**3** are listed in Table 2. The almost identical dissymmetric ligand geometry with respect to the N−H and N side between **1**·DMF and **1**·DMAC supports the cis/trans assignment of the protonation sites in **1**·DMAC.

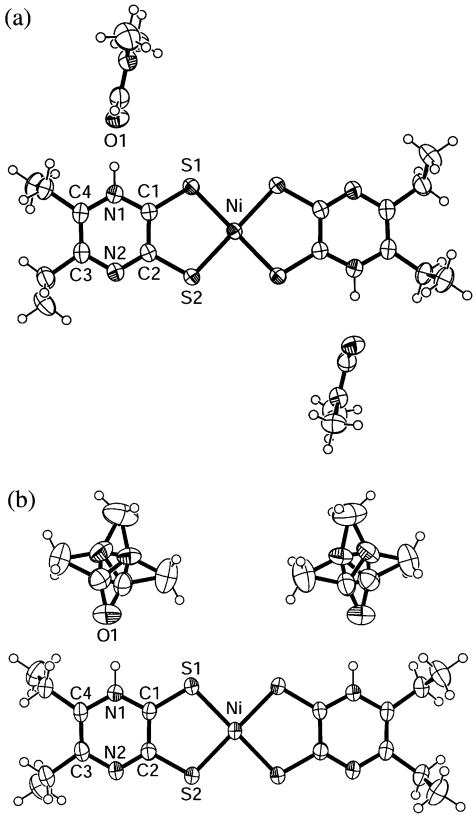

Figure 1. ORTEP drawings of **1** with thermal ellipsoids drawn at 50% probability: (a) **1**·2DMF; (b) **1**·2DMAC. DMAC molecules are disordered.

The Ni complex **1**·2DMF gives an intrachelate S−Ni−S angle of 92.75(3)° and almost identical Ni−S bond lengths (2.1680(9) and 2.1714(9) Å). These Ni−S bond lengths are very close to those of $[Ni(S_2C_2Me_2)_2]^{2-}$ with Ni(II) formulation (2.179(4) Å).[7] The S−C and N−C distances of **1**·2DMF exhibit some differences on the N−H and N side. A similar trend is also observed in the case of **1**·2DMAC. These differences in bond lengths, i.e., bond alternation, suggest a large contribution of the following monoanionic structure to the electronic structure of the ligand:

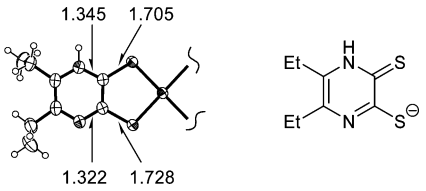

Thus, the oxidation state of the Ni atom of **1** is +II. Such characteristics in the geometry of the ligands are also found in the other complexes such as **2** and **3**. Therefore, we can assign the oxidation state as +II for Pd and Pt. To confirm the assignment, a quantum chemical calculation of **1** was performed by the DFT method (RB3LYP/LANL2DZ). Figure 2 shows the molecular orbital diagram of **1** along with that of $Ni^{III}(HL)(L)$ and $Ni^{IV}(L)_2$. The natural population analysis based on DFT calculations gives 9.07 electrons on

(4) Mitani has reported the fascinating function for hydrogen-bonded charge-transfer complexes, i.e., proton motion with a high frequency, quantum proton fluctuation, and strong proton−electron interaction. See: Mitani, T.; Inabe, T. In *Advances in Spectroscopy*; Clark, R. J. H., Hester, R. E., Eds.; John Wiley & Sons: Chichester, U.K., 1993; Vol. 22, pp 291−331.

(5) Robertson, N.; Cronin, L. *Coord. Chem. Rev.* **2002**, *227*, 93−127.

(6) Becher, J.; Stidsen, C. E.; Toftlund, H.; Asaad, F. M. *Inorg. Chim. Acta* **1986**, *121*, 23−26.

(7) Lim, B. S.; Fomitchev, D. V.; Holm, R. H. *Inorg. Chem.* **2001**, *40*, 4257−4262.

Table 1. Crystallographic Data for **1**−**3**

	1·2DMF	**1**·2DMAC	**2**·2DMAC	**3**·2DMAC
formula	$C_{22}H_{36}N_6S_4NiO_2$	$C_{24}H_{40}N_6NiO_2S_4$	$C_{24}H_{40}N_6PdO_2S_4$	$C_{24}H_{40}N_6PtO_2S_4$
fw	603.51	631.57	679.26	767.95
color and habit	brown, block	brown, prism	red, prism	violet, block
cryst system	triclinic	monoclinic	monoclinic	monoclinic
space group	$P\bar{1}$ (No. 2)	$C2/c$ (No. 15)	$C2/c$ (No. 15)	$C2/c$ (No. 15)
a (Å)	8.1157(5)	16.0698(2)	16.016(3)	15.91(2)
b (Å)	9.1057(8)	12.2833(5)	12.251(4)	12.227(9)
c (Å)	10.794(1)	15.6376(2)	15.786(2)	15.75(1)
α (deg)	72.092(2)			
β (deg)	68.350(2)	97.771(3)	97.11(1)	97.07(3)
γ (deg)	88.225(4)			
V (Å^3)	702.4(1)	3058.4(1)	3074(1)	3040(5)
Z	1	4	4	4
T (°C)	−73	23	23	23
μ(Mo Kα) (cm^{-1})	1.019	0.939	0.907	4.923
D_{calcd} (g cm^{-3})	1.427	1.372	1.468	1.678
reflcns measd	6074	13902	3516	3475
reflcns used	2446	2081	2278	2485
params	160	186	186	186
R1, wR2 [$I > 2\sigma(I)$]	0.066, 0.165	0.051, 0.116	0.034, 0.088	0.037, 0.067
GOF on F^2	0.999	1.003	0.966	0.850

Table 2. Selected Bond Lengths and Angles for **1**−**3**

	1·2DMF	**1**·2DMAC	**2**·2DMAC	**3**·2DMAC
M−S(1)	2.1680(9)	2.181(1)	2.306(1)	2.305(2)
M−S(2)	2.1714(9)	2.174(1)	2.289(1)	2.285(2)
S(1)−C(1)	1.705(4)	1.706(3)	1.703(3)	1.705(5)
S(2)−C(2)	1.728(4)	1.736(3)	1.736(3)	1.731(5)
C(1)−C(2)	1.416(5)	1.420(5)	1.433(5)	1.423(6)
C(1)−N(1)	1.345(5)	1.347(4)	1.344(4)	1.344(5)
C(2)−N(2)	1.322(5)	1.321(4)	1.319(4)	1.322(5)
N(1)−O(1)	2.685(4)	2.765(4)	2.736(4)	2.751(5)
S(1)−M−S(2)	92.75(3)	92.15(3)	89.54(3)	89.63(7)

the 3d orbital of the Ni atom, indicating a d^8 configuration with a charge transfer from the ligands to the nickel metal.[8]

Table 3 shows the electronic absorption bands of M(HL)$_2$. All the neutral complexes gave intense bands in the range of 400−700 nm (Figure S1), which could be assigned to the HOMO(ψ_{62}, b_g) → LUMO(ψ_{63}, a_u) transition. The TD-DFT (RB3LYP/LANL2DZ) calculation for Ni(HL)$_2$ suggested a low-energy band with an oscillator strength of 0.282 at 550 nm corresponding to the HOMO → LUMO transition. The DFT calculation shows that the HOMO possesses large coefficients on the ligands with a nonnegligible metal contribution, whereas the LUMO localizes on the ligands. The distribution pattern of the frontier orbitals indicates that the low-energy intense band observed in M(HL)$_2$ can be assigned to the MMLLCT (mixed metal−ligand to ligand CT).[9] These intense bands give the order of increasing energy as Ni ≈ Pt < Pd, which is in accordance with the behavior of the transition energies of the square planar M(SST)$_2$ complexes.[10] The anomalous behavior of the Pd complexes is also seen in the optical and electrochemical properties of the M(bpy)(bdt) complexes.[9b]

Electrochemical Behavior of Proton and Electron Donors 1−3. Cyclic voltammetry of **1**−**3** in DMF gave two irreversible redox waves. The lack of reversibility in the first redox wave (Table 4) appears to be related to the coupling of the proton transfer process and the redox process. This is because the corresponding dianionic species (**1**$^{2-}$−**3**$^{2-}$) show fully reversible behavior in the dianion/monoanion redox process. The first oxidation potentials, E_1^{ox}, imply that the electron donor abilities of **1**−**3** are comparable to that of tetrathiafulvalene (TTF).[11] The irreversibility in the second redox process could be caused by the intrinsic instability of highly oxidized species because the dianion **1**$^{2-}$−**3**$^{2-}$ species gave irreversible redox waves in the monoanion/neutral redox process.

In general, the redox reaction coupled to the proton transfer is referred to as the proton-coupled electron transfer (PCET).[1a,b,3,12] The PCET reaction of many metal−ligand systems having dissociative protons has been widely studied by pH-dependent cyclic voltammetry to estimate redox potentials and acid dissociation constants. Therefore, the redox potentials of **1**−**3** were monitored in the pH range of 2−10 in 3:1 (v/v) acetonitrile−aqueous solution. Figure 3 shows the Pourbaix diagram for **1**. The cyclic voltammogram of **1** clearly revealed a pH dependence. The pH dependence of these redox couples was fitted using the following equations:

$$E_{II/III} = E^{\circ\prime}_{II/III} - 0.059[\log(K_a^{III} + [H^+]) - \log(K_{a1}^{II}K_{a2}^{II} + K_{a1}^{II}[H^+] + [H^+]^2)] \quad (1)$$

$$E_{III/IV} = E^{\circ\prime}_{III/IV} + 0.059[\log(K_a^{III} + [H^+])] \quad (2)$$

Here $E^{\circ\prime}_{II/III}$ and $E^{\circ\prime}_{III/IV}$ are the formal standard redox potentials of the Ni(II)/Ni(III) and Ni(III)/Ni(IV) couples at pH = 0, respectively, and K_{a1}^{II}, K_{a2}^{II}, and K_a^{III} are the acid dissociation constants for Ni^{II}(HL)$_2$, Ni^{II}(HL)(L)$^-$, and Ni^{III}-

(8) Bachler, V.; Olbrich, G.; Neese, F.; Wieghardt, K. *Inorg. Chem.* **2002**, *41*, 4179−4193.
(9) (a) Paw, W.; Cummings, S. D.; Mansour, M. A.; Connick, W. B.; Geiger, D. K.; Eisenberg, R. *Coord. Chem. Rev.* **1998**, *171*, 125−150. (b) Cocker, T. M.; Bachman, R. E. *Inorg. Chem.* **2001**, *40*, 1550−1556.
(10) Forbes, C. E.; Holm, R. H. *J. Am. Chem. Soc.* **1970**, *92*, 2297−2303.
(11) The oxidation potential of TTF was +0.08 V (vs Fc/Fc$^+$) in DMF.
(12) (a) Thorp, H. H. *Chemtracts: Inorg. Chem.* **1991**, *3*, 171−184. (b) Stubbe, J.; Nocera, D. G.; Yee, C. S.; Chang, M. C. Y. *Chem. Rev.* **2003**, *103*, 2167−2201.

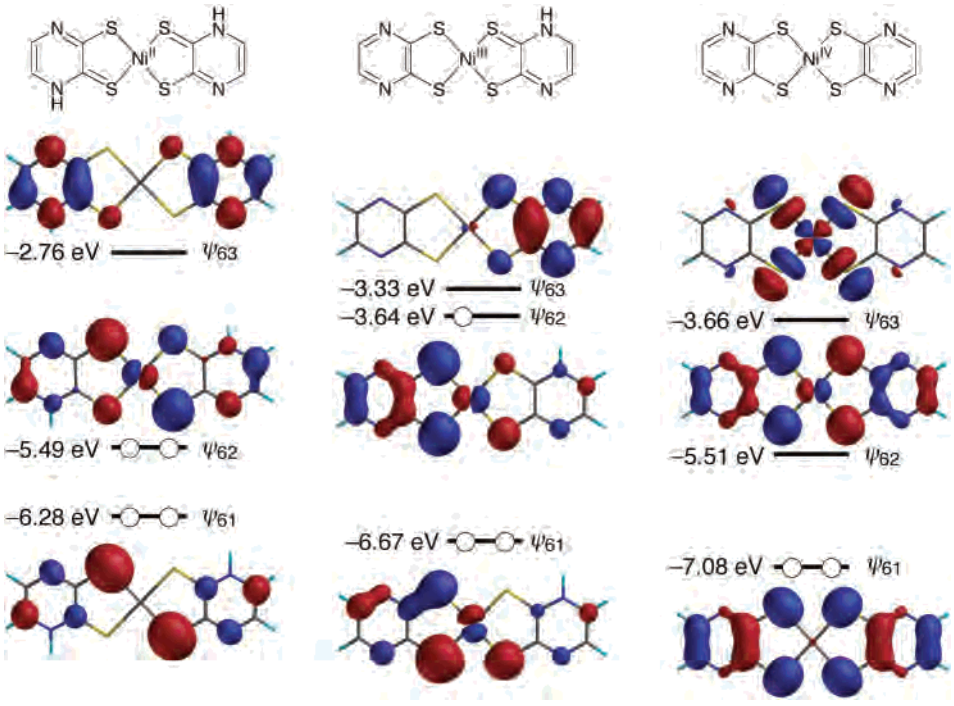

Figure 2. Molecular orbitals of nonsubstituted $Ni^{II}(HL)_2$, $Ni^{III}(HL)(L)$, and $Ni^{IV}(L)_2$ based on the R(O)B3LYP/LANL2DZ calculation.

Table 3. Electronic Transition Data for **1**−**3**

$Ni(HL)_2$ (**1**)	$Pd(HL)_2$ (**2**)	$Pt(HL)_2$ (**3**)
299 (28 000)	277 (18 200)	337 (6400)
354 (20 400)	385 (4800)	414 (3200)
592 (11 300)	502 (7600)	591 (8200)
	527 (7700)	

(HL)(L), respectively.[3c] The best fitting curves were obtained with the values listed in Table 5.[13] According to the equations, the potential of the Ni(II) (red area)/Ni(III) (green area) couple is dependent on pH below approximately 8 with an initial slope of −60 mV/pH unit. The slope gradually increases to a maximum of −120 mV/pH unit near pH ∼ 6 and remains constant until pH ∼ 4, where it decreases again to approximately −60 mV/pH unit. On the other hand, the potential of the Ni(III) (green)/Ni(IV) (blue) couple exhibits a pH-independent behavior above pH ∼ 4 and increases with a slope of −60 mV/pH below pH ∼ 4.[14]

Equilibrium Constants for Proton and Electron Transfer Reactions. The comproportionation equilibrium constants, K_{com}, for the following PCET reaction were obtained from the difference in the standard redox potentials, i.e., $K_{com} = \exp(-\Delta G^{\circ}_{com}/RT)$, where $\Delta G^{\circ}_{com} = -nF\Delta E^{\circ}_{com}$ and $\Delta E^{\circ}_{com} = E^{\circ\prime}_{III/IV} - E^{\circ\prime}_{II/III}$:

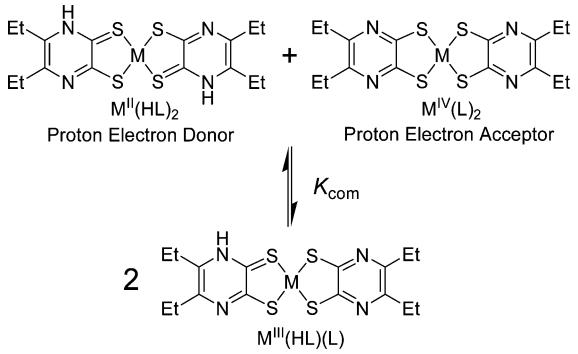

The proton and electron transfer reaction between $Ni^{II}(HL)_2$ and $Ni^{IV}(L)_2$ favors the forward direction (K_{com} = 2500) at 25 °C for pH < 4 in contrast to the backward direction found in the hydroquinone−benzoquinone system.[15] This finding suggests that the charge-transfer complex between $Ni^{II}(HL)_2$ and $Ni^{IV}(L)_2$ could transfer to the PET state under milder conditions in the solid state than in the hydroquinone−benzoquinone system. The thermodynamic stability of the PET state for the $Ni^{II}(HL)_2$−$Ni^{IV}(L)_2$ system was supported using DFT calculations, which indicate that the proton and electron transfer reactions are exo- and endothermic for the $Ni^{II}(HL)_2$−$Ni^{IV}(L)_2$ system (−10.5 kJ/mol) and the hydroquinone−benzoquinone system (+81.1 kJ/mol), respectively. Although the other complexes such as **2** and **3** also exhibit $K_{com} > 1$, the thermodynamic stability of the PET states is small in comparison with that of **1**. In contrast to our results, Lappin reported the thermodynami-

(13) The differences in the oxidation potentials between E_1^{ox} (in Table 4) and $E^{o\prime}_{II/III}$ (in Table 5) should arise from the differences of the solvent used in the CV measurements. The potential differences of 0.24−0.32 V are similar to those of the reported values of hydroquinones in various solvents. See reaction 6 in Table 1 of the following reference: Stallings, M. D.; Morrison, M. M.; Sawyer, D. T. *Inorg. Chem.* **1981**, *20*, 2655−2660.

(14) The pH-dependent CV was measured under the condition of 3:1 acetonitrile−water solutions of the complexes due to the solubility limitation of the complexes in aqueous solution. Because the glass electrode pH meter gives a reproducibly Nernstian response to hydrogen ion concentration in aqueous, acetonitrile, and their mixed solutions, the apparent pH values obtained directly from the meter readings in 3:1 acetonitrile−water solutions were referred to as pH. See: Rondinini, S.; Mussini, P. R.; Mussini, T. *Pure Appl. Chem.* **1987**, *59*, 1549−1560.

(15) Patai, S.; Rappoport, Z. *The chemistry of the quinonoid compounds*; Wiley: New York, 1988; Vol. 2, Part 1, p 719.

Table 4. Oxidation Potentials of Neutral Species **1**−**3** and Dianion Species $\mathbf{1}^{2-}$−$\mathbf{3}^{2-}$ [a]

	1	2	3	$\mathbf{1}^{2-}$	2^{2-}	3^{2-}
E_1^{ox}	−0.10[b]	+0.13[b]	−0.04[b]	−0.64[c]	−0.38[c]	−0.61[c]
E_2^{ox}	+0.28[b]	+0.28[b]	+0.26[b]	+0.21[b]	+0.18[b]	+0.10[b]

[a] See Experimental Section for measurement conditions. [b] E_{pa}. [c] $E_{1/2}$.

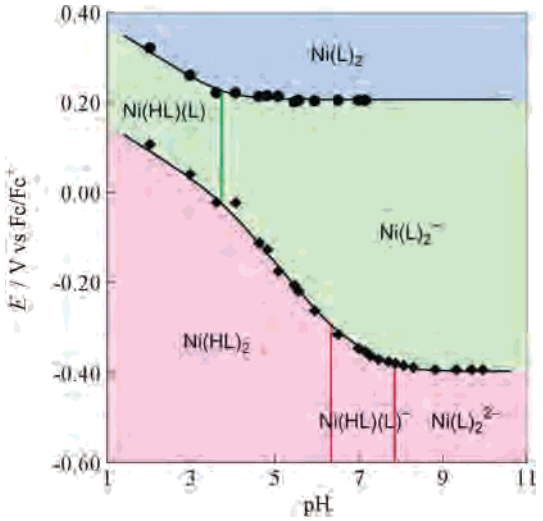

Figure 3. Pourbaix diagram of **1**. Red, green, and blue areas correspond to formal Ni(II), Ni(III), and Ni(IV) oxidation states, respectively.

Table 5. Parameters for the pH-Dependent CV Measurement of **1**−**3**[a]

	$E^{o}_{II/III}$	$E^{o\prime}_{III/IV}$	K_{com}	pK_{a1}^{II}	pK_{a2}^{II}	pK_{a}^{III}	pK_{a1}^{II} [b]	pK_{a2}^{II} [b]
1	+0.22	+0.42	2500	6.5	7.6	3.6	6.1	7.8
2	+0.40	+0.44	4.8	6.0	7.3	3.6	5.8	7.8
3	+0.20	+0.33	160	6.1	7.7	4.1	5.8	7.8

[a] See Experimental Section for measurement conditions. [b] Determined by spectrophotometric titration of **1**−**3**.

cally favored disproportionation reaction of the $Ni^{III}L'H^{2+}$ complex [$L'H_2$ = bis(oxime imine)].[16] This discrepancy could be attributed to the difference in the degree of spin delocalization onto the ligands. The unpaired electron on the Ni(III) atom of $Ni^{III}(HL)(L)$ can widely delocalize on the sp^2-based ligand through LMCT and can minimize an excess positive charge on the Ni atom. Such a highly delocalized structure would lead to the thermodynamically favored comproportionation reaction in the $M^{II}(HL)_2$−$M^{IV}(L)_2$ system (Figure 4). This valence bond picture is supported by the DFT calculation of the Ni(III) species indicating a wide-spreading SOMO (ψ_{62}) on the entire molecule (Figure 2). Another possible mechanism for the discrepancy between Lappin's and our system is the electrostatic differences between a thiolate ion and an N_2O_2 system. It is well-known that the stabilization of the high-oxidation Ni species requires ligands with high electron densities. Most well-characterized Ni(IV) complexes contain N, O, and F donor atoms. The thiolate ion can be regarded as a soft nucleophile, which less stabilizes the Ni(IV) oxidation states than a hard N_2O_2 system in the context of the soft−hard acid−base theory.[17]

Proton donor ability of **1**−**3** can also be estimated from the Pourbaix diagram. Acid dissociation constants obtained from the curve fitting gave small pK_{a1}^{II} values, which were consistent with the weak acid character of the donor **1**−**3**. The almost identical acidity within **1**−**3** indicates that the metal redox ability has a small influence on the acidity of the ligands. Spectrophotometric titration (Figure S2) of **1**−**3** supported the acid dissociation constants obtained from the Pourbaix diagram. At first glance, the invariance of the pK_a values among **1**−**3** seems to indicate that the redox process is ligand-centered rather than metal-centered. However, this idea is inconsistent with the difference in the redox potentials of **1**−**3** and with the 20−27% metal character of the molecular orbitals. Thus, the redox reactions should mainly be ligand-centered with a small but nonnegligible contribution of metal atoms.

Synthesis and Properties of Proton and Electron Acceptor 4. Cyclic voltammetry of dianion $M(L)_2^{2-}$ $\mathbf{1}^{2-}$−$\mathbf{3}^{2-}$ in CH_2Cl_2 gave reversible and irreversible redox waves in the first and second redox processes, respectively (Table 4). The second oxidation potentials, E_2^{ox}, imply that the electron acceptor ability of formal M(IV) oxidation states, i.e., neutral $M^{IV}(L)_2$, should be comparable to that of 2,3-dichloro-5,6-dicyano-*p*-benzoquinone (DDQ).[18] The oxidation of the dianion species $\mathbf{1}^{2-}$−$\mathbf{3}^{2-}$ with 1 equiv of I_2 afforded dark green solutions showing intense ESR signals.[19] The anisotropic *g*-values for these Ni, Pd, and Pt complexes were similar to those for most square planar dithiolate complexes of M(III) formulation.[20] This finding indicates that the one-electron oxidized species of $\mathbf{1}^{2-}$−$\mathbf{3}^{2-}$ are of $M^{III}(L)_2^-$ type. Further oxidation of $M^{III}(L)_2^-$ is expected to give $M^{IV}(L)_2$ as a proton and electron acceptor. However, several attempts to obtain $Ni^{IV}(L)_2$ and $Pd^{IV}(L)_2$ have so far been unsuccessful. On the other hand, the oxidation of $Pt^{II}(L)_2^{2-}$ with excess DDQ successfully afforded dark blue microcrystalline powders. IR, FAB-mass spectroscopy, and elemental analysis supported the generation of $Pt^{IV}(L)_2$ (**4**). The UV spectrum of **4** in CH_2Cl_2 exhibited deviations from Beer's law, which is consistent with the formation of a dimer and partial dissociation into the monomeric species (Figure 5). The TD-DFT calculation for $Pt^{IV}(L)_2$ predicts an intense absorption band at 734 nm derived from a HOMO−LUMO transition, indicating that the band observed at 826 nm is an intramolecular transition of the monomeric $Pt^{IV}(L)_2$. The dimeric character was also supported by the FAB-mass spectrum (Figure S4) of **4**, which gave additional peaks of *m*/*z* 985

(16) Lappin, A. G.; Martone, D. P.; Osvath, P. *Inorg. Chem.* **1985**, *24*, 4187−4191.
(17) (a) Pearson, R. G. *J. Am. Chem. Soc.* **1963**, *85*, 3533−3539. (b) Pearson, R. G.; Songstad, J. *J. Am. Chem. Soc.* **1967**, *89*, 1827−1836.
(18) The reduction potential of DDQ was +0.11 V (vs Fc/Fc^+) in CH_2Cl_2.
(19) *g*-values observed in CH_2Cl_2 at −120 °C: $Ni^{III}(L)_2^-$, 2.186, 2.046, 2.026; $Pd^{III}(L)_2^-$, 2.073, 2.041, 1.950; $Pt^{III}(L)_2^-$, 2.225, 2.051, 1.979. See also Figure S3.
(20) (a) Davison, A.; Edelstein, N.; Holm, R. H.; Maki, A. H. *Inorg. Chem.* **1964**, *3*, 814−823. (b) Lim, B. S.; Fomitchev, D. V.; Holm, R. H. *Inorg. Chem.* **2001**, *40*, 4257−4262.

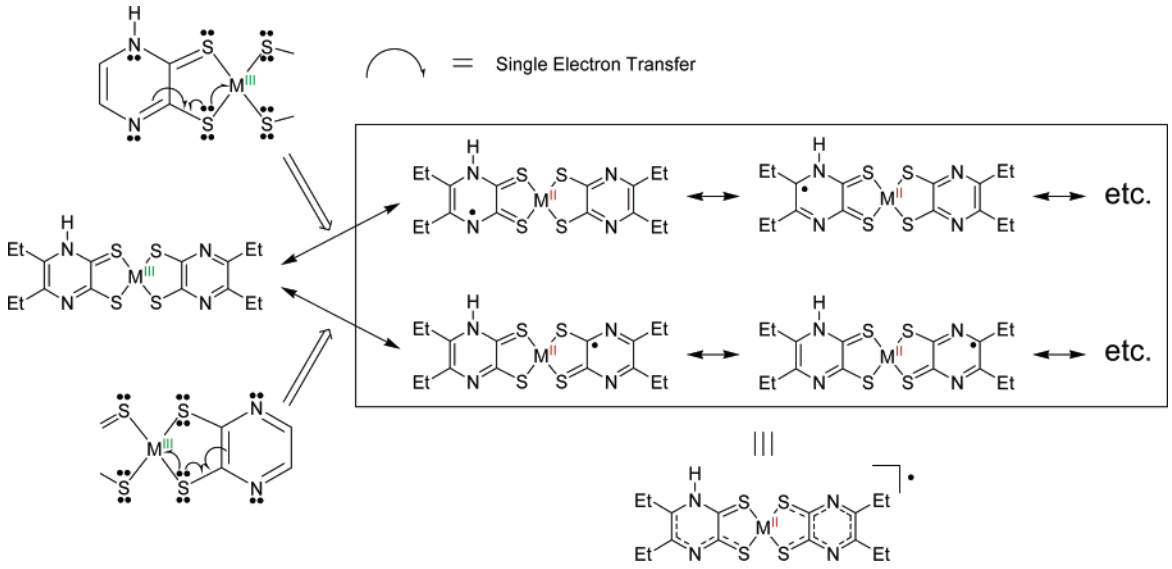

Figure 4. Valence bond diagram for spin delocalization of $M^{III}(HL)(L)$.

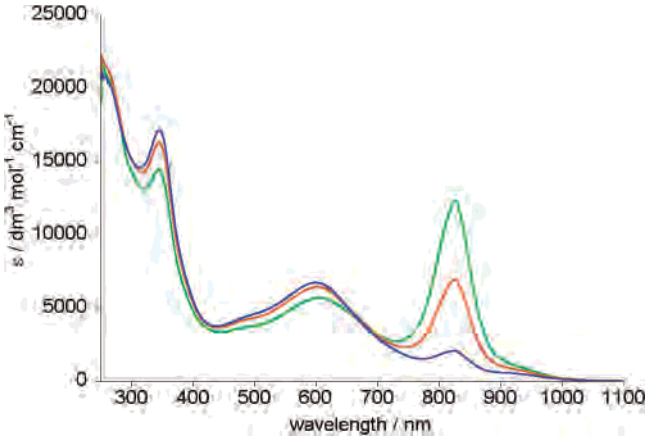

Figure 5. Electronic absorption spectra of $Pt^{IV}(L)_2$ at various concentrations: green line, 1.64×10^{-5} mol/L; orange line, 3.28×10^{-5} mol/L; blue line, 1.64×10^{-4} mol/L.

and 1184 that originated from the $[2M - L + H]^+$ and $[2M + H]^+$ species, respectively.[21] It is noted that dianion species $\mathbf{3}^{2-}$ can lead to both a good neutral electron donor and a good neutral electron acceptor in *one* step (protonation of **3** and oxidation of **4**, respectively).

Conclusion

We obtained $M^{II}(HL)_2$ (M = Ni, Pd, Pt) as a proton and electron donor and investigated the thermodynamic driving force associated with the coupling of proton and electron transfer. Furthermore, we also succeeded in the generation of $Pt^{IV}(L)_2$ as a proton and electron acceptor. As expected, the proton and electron transfer state of the $M^{II}(HL)_2-M^{IV}(L)_2$ system was more thermodynamically stabilized in comparison with that of the hydroquinone−benzoquinone system. Currently, we are investigating the solid-state properties of the charge-transfer complex between $Pt^{II}(HL)_2$ and $Pt^{IV}(L)_2$.

(21) For characterization of a dimeric dithiolene complex, see: Balch, A. L.; Dance, G. I.; Holm, R. H. *J. Am. Chem. Soc.* **1968**, *90*, 1139−1145.

Experimental Section

All experiments with moisture- or air-sensitive compounds were performed in anhydrous solvents under an argon atmosphere in well-dried glassware. The solvents were dried and distilled according to the standard procedures. The infrared and electronic spectra were recorded using a Perkin-Elmer FT 1640 IR spectrometer and a Shimadzu UV-3100PC spectrometer, respectively. The ^{1}H NMR and ESR spectra were obtained using a JEOL EX-270 spectrometer and a JEOL JES-FE2XG spectrometer, respectively.

The cyclic voltammetric measurements were performed with a ALS-612A electrochemical analyzer using a glassy carbon working electrode, a Pt counter electrode, and an $Ag/AgNO_3$ reference electrode in DMF (for **1**−**3**) or CH_2Cl_2 (for **4**−**6**) containing 0.1 M Bu_4NClO_4 as the supporting electrolyte at a scan rate of 100 mV/s. The Fc/Fc^+ couple was used as an internal standard. For pH-dependent CV measurements, a glassy carbon working electrode, a Pt counter electrode, and an $Ag/AgNO_3$ reference electrode were used in CH_3CN/H_2O (3:1, v/v) containing 0.1 M Bu_4NClO_4 as the supporting electrolyte at a scan rate of 100 mV/s. The Fc/Fc^+ couple was used as an internal standard. The pH measurements were carried out using a HORIBA F-24C pH meter. The parameters of the pH-dependent CV measurements were determined by the least-squares curve fitting on the basis of eqs 1 and 2.

Synthesis of $M(HL)_2$ (1−3). The mixture of 2,3-diethyl-5,6-bis(2-methyl-2-propylthio)pyrazine (1 g, 3.2 mmol), metal source (1.6 mmol), and three drops of concentrated hydrochloric acid in 2-methoxyethanol (25 mL) was refluxed for 12 h. The solvent was evaporated, and the resultant blue powders were washed with water. Recrystallization from the DMF solution yielded dark violet crystals. **1**: mp >300 °C; IR (KBr, cm^{-1}) 2966, 2935, 1645, 1154, 1047, 675; ^{1}H NMR (270 MHz, NaOD/D_2O/DMSO-d_6) δ 1.017 (12H), 2.414 (8H); ^{13}C NMR (67.8 MHz, NaOD/D_2O/DMSO-d_6) δ 15.21, 26.27, 142.71, 166.56. Anal. Found: C, 43.54; H, 5.97; N, 13.90; S, 20.83. Calcd for $C_{22}H_{36}N_6NiO_2S_4$: C, 43.78; H, 6.01; N, 13.93; S, 21.25. **2**: mp >300 °C; IR (KBr, cm^{-1}) 2966, 2935, 1645, 1154, 1047, 675; ^{1}H NMR (270 MHz, NaOD/D_2O/DMSO-d_6) δ 1.010 (12H), 2.452 (8H); ^{13}C NMR (67.8 MHz, NaOD/D_2O/DMSO-d_6) δ 15.71, 27.02, 145.06, 170.16. Anal. Found: C, 40.37; H, 5.49; N, 12.89; S, 19.51. Calcd for $C_{22}H_{36}N_6O_2PdS_4$: C, 40.57; H, 5.57; N, 12.90; S, 19.70. **3**: mp >300 °C; IR (KBr, cm^{-1}) 2967, 2935, 1646, 1155, 1046, 676; ^{1}H NMR (270 MHz, NaOD/D_2O/DMSO-

d_6) δ 1.024 (12H), 2.453 (8H); ^{13}C NMR (67.8 MHz, NaOD/D_2O/DMSO-d_6) δ 15.32, 26.80, 143.70, 168.98. Anal. Found: C, 35.44; H, 4.69; N, 11.28; S, 17.16. Calcd for $C_{22}H_{36}N_6O_2PtS_4$: C, 35.71; H, 4.90; N, 11.36; S, 17.34.

Synthesis of $(Bu_4N)_2Pt(L)_2$. An aqueous solution of Bu_4NBr (435 mg, 1.35 mmol) was added to a solution of $Pt(HL)_2$ (**3**) (400 mg, 0.674 mmol) in an aqueous NaOH solution (1 mol/L, 15 mL). The resultant vivid yellowish orange powder was collected by filtration and washed with a small amount of water. Yield: 648 mg (89%). Anal. Found: C, 53.00; H, 8.48; N, 7.80. Calcd for $C_{48}H_{92}N_6PtS_4$: C, 53.55; H, 8.61; N, 7.81. ^{1}H NMR (270 MHz, CF_3COOD):[22] δ 0.923 (24H), 1.280 (16H), 1.386 (8H), 2.770 (8H), 3.087 (16H).

Synthesis of $Pt(L)_2$ (4). The dianion species $(Bu_4N)_2Pt(L)_2$ (255 mg, 0.237 mmol) and DDQ (210 mg, 0.925 mmol) were dissolved in 10 mL of CH_2Cl_2. The mixture was stirred for 2 h at room temperature. After evaporation of the solvent, the resultant dark blue powder was washed with acetone. Recrystallization from benzene solution yielded a dark blue microcrystalline powder **4**.[23] Yield: 110.9 mg (79%). Mp: >300 °C. IR (KBr, cm^{-1}): 2970, 2933, 1495, 1444, 1360, 1299 1202, 1157, 1042. MS (FAB, NBA): *m*/*z* 591 [$(M + H)^+$]. Anal. Found: C, 32.21; H, 3.42; N, 9.29. Calcd for $C_{16}H_{20}N_4PtS_4$: C, 32.48; H, 3.41; N, 9.47. UV-(CH_2Cl_2, nm): 344, 606, 826.

X-ray Crystallography. Data collection was performed using a Rigaku RAXIS-RAPID Imaging plate diffractometer (Mo Kα, λ = 0.710 69 Å) for **1**·2DMF, **1**·2DMAC, and **3**·2DMAC and using a Rigaku AFC5R (Mo Kα, λ = 0.710 69 Å) for **2**·2DMAC. The structure was solved with direct methods and refined by the full-matrix least-squares method (SHELX-97) on F^2. All the non-hydrogen atoms were refined anisotropically. The hydrogen atoms were placed in their calculated positions. The crystallographic details are summarized in Table 1.

Computational Details. All the DFT calculations of the metal complexes were performed at the B3LYP/LANL2DZ level using the Gaussian 98 program.[24] Geometry optimizations were carried out with C_{2h} for $Ni^{II}(HL)_2$, C_s for $Ni^{III}(HL)(L)$, and D_{2h} symmetry for $Ni^{IV}(L)_2$. The time-dependent DFT (TD-DFT) calculation of $Ni^{II}(HL)_2$ was done with the atom positions determined by the X-ray crystallographic analysis. The TD-DFT calculation for $Pt^{IV}(L)_2$ was performed with D_{2h}-optimized geometry.

Supporting Information Available: Figures showing UV, ESR, and FAB-mass spectra and spectrophotometric titration and crystallographic data in CIF format. This material is available free of charge via the Internet at http://pubs.acs.org.

IC049621+

(22) ^{1}H NMR of $(Bu_4N)_2Pt(L)_2$ in $CDCl_3$ caused signal broadening due to a trace amount of open-shell $Pt(L)_2^-$, which would be generated by air oxidation. The solution of $(Bu_4N)_2Pt(L)_2$ in CH_2Cl_2 initially gives the reddish orange color, which gradually turned to green in air. The newly appeared band in the UV spectra is identical with that of $Pt(L)_2^-$ generated by one-electron oxidation of $(Bu_4N)_2Pt(L)_2$ with I_2.

(23) ^{1}H NMR (270 MHz, CD_2Cl_2) of **4** gave two broad signals at δ 1.09 and 2.57 in the temperature range from +30 to −50 °C.

(24) Frisch, M. J.; Trucks, G. W.; Schlegel, H. B.; Scuseria, G. E.; Robb, M. A.; Cheeseman, J. R.; Zakrzewski, V. G.; Montgomery, J. A., Jr.; Stratmann, R. E.; Burant, J. C.; Dapprich, S.; Millam, J. M.; Daniels, A. D.; Kudin, K. N.; Strain, M. C.; Farkas, O.; Tomasi, J.; Barone, V.; Cossi, M.; Cammi, R.; Mennucci, B.; Pomelli, C.; Adamo, C.; Clifford, S.; Ochterski, J.; Petersson, G. A.; Ayala, P. Y.; Cui, Q.; Morokuma, K.; Malick, D. K.; Rabuck, A. D.; Raghavachari, K.; Foresman, J. B.; Cioslowski, J.; Ortiz, J. V.; Baboul, A. G.; Stefanov, B. B.; Liu, G.; Liashenko, A.; Piskorz, P.; Komaromi, I.; Gomperts, R.; Martin, R. L.; Fox, D. J.; Keith, T.; Al-Laham, M. A.; Peng, C. Y.; Nanayakkara, A.; Gonzalez, C.; Challacombe, M.; Gill, P. M. W.; Johnson, B. G.; Chen, W.; Wong, M. W.; Andres, J. L.; Head-Gordon, M.; Replogle, E. S.; Pople, J. A. *Gaussian 98*; Gaussian, Inc.: Pittsburgh, PA, 1998.